Experimental Mechanics
https://doi.org/10.1007/s11340-019-00520-4

Application of Digital Image Correlation (DIC) to the Measurement of Strain Concentration of a PVA Dual-Crosslink Hydrogel Under Large Deformation

M. Liu [1] · J. Guo [1] · C.-Y. Hui [1] · A.T. Zehnder [1]

Received: 29 October 2018 / Accepted: 17 April 2019

Abstract

Hydrogels are a class of soft, highly deformable materials formed by swelling a network of polymer chains in water. With mechanical properties that mimic biological materials, hydrogels are often proposed for load bearing biomedical or other applications in which their deformation and failure properties will be important. To study the failure of such materials a means for the measurement of deformation fields beyond simple uniaxial tension tests is required. As a non-contact, full-field deformation measurement method, Digital Image Correlation (DIC) is a good candidate for such studies. The application of DIC to hydrogels is studied here with the goal of establishing the accuracy of DIC when applied to hydrogels in the presence of large strains and large strain gradients. Experimental details such as how to form a durable speckle pattern on a material that is 90% water are discussed. DIC is used to measure the strain field in tension loaded samples containing a central hole, a circular edge notch and a sharp crack. Using a nonlinear, large deformation constitutive model, these experiments are modeled using the finite element method (FEM). Excellent agreement between FEM and DIC results for all three geometries shows that the DIC measurements are accurate up to strains of over 10, even in the presence of very high strain gradients near a crack tip. The method is then applied to verify a theoretical prediction that the deformation field in a cracked sample under relaxation loading, i.e. constant applied boundary displacement, is stationary in time even as the stress relaxes by a factor of three.

Keywords Digital image correlation · Hydrogel · Large deformation · Finite element simulation · Viscoelastic · Crack tip field

Introduction

A hydrogel is essentially a network of polymer chains swollen in water. Due to similarities in physical properties with biological tissues, hydrogels have potential applications in biomedical engineering, such as artificial cartilage [1] and as vehicles for drug delivery [2]. However, conventional hydrogels are too brittle to be used for load carrying applications. Researchers have been able to overcome this limitation using the idea of double, interpenetrating networks [3–6]. The first network serves as a sacrificial network; it breaks under load and dissipates energy. The second network is highly extensible; it prevents the growth of cracks. A drawback of the first generation of these gels is that the damage in the sacrificial network is irreversible. To overcome this, researchers have introduced non-covalent, transient crosslinks in the sacrificial network [5, 6]. These transient bonds can break and reform. As a result, the hydrogel is able to sustain large deformations and to recover to its original state after unloading. These gels exhibit complex, rate dependent behavior which is still not well understood. There is, however, a simple system where the mechanical behavior can be accurately modeled by continuum theory. This system is the PVA dual-crosslink gel developed by Mayumi et al. [7]. The understanding of the mechanical behavior of this system is beneficial to the study of more complex systems. Long et al. [8] and Guo et al. [9] have developed a 3D constitutive model for this hydrogel which can accurately capture the material response in uniaxial tension [8, 9] and cyclic shear tests [10] and correctly predicts the crack opening displacement in edge cracked samples loaded in tension [11]. Liu et al. [12] studied the effects of temperature and loading rates on the mechanical response and find that classical time temperature superposition is applicable to this hydrogel.

✉ A. T. Zehnder
atz2@cornell.edu

[1] Sibley School of Mechanical and Aerospace Engineering, Field of Theoretical & Applied Mechanics, Cornell University, Ithaca, NY 14853, USA

Published online: 30 April 2019

A good understanding and the ability to model of the mechanical behaviors of such materials is critical to facilitate practical applications. The above-mentioned tests, involving uniaxial tension and cyclic shear tests, measure the homogenous deformation material response. However, they cannot probe the response of the material in the presence of cracks or other stress concentrators, which is important for problems such as contact and fracture prediction. As a non-contact, full-field deformation measurement method, Digital Image Correlation (DIC) is an ideal candidate for the measurement of inhomogeneous deformation of hydrogels. DIC measures deformation by tracking the position change of a group of pixels (subset) from the images corresponding to undeformed and deformed states. 2D DIC measures planar motion and requires only one camera. The details of 2D DIC can be found in Pan et al. [13], Khoo et al. [14] and Schreier et al. [15].

Several researchers have applied 2D DIC (referred to here as simply DIC) to study the material response of soft materials such as gels in the presence of strain concentrations. For instance, Kwon et al. [16] evaluated the stress–strain relationship, strain localization and Poisson's ratio of agarose gel using DIC. In their experiment, a small notch was made on the agarose gel specimen, and the strain close to the notch was measured with DIC. This strain was characterized as the failure strain of the material. Sasson et al. [17] used DIC to measure the surface strain induced by a spherical tip indenter indenting chitosan hydrogels. The results were used to demonstrate the capability of their constitutive model. Leibinger et al. [18] used a laser-based image correlation method to measure the displacement and strain fields induced during the insertion of a needle into soft tissue phantoms. Hong et al. [19] applied DIC in their investigation of bubble cavitation damage to a tissue surrogate. Christensen et al. [20] implemented DIC to determine the local strain distribution within 3D printed hydrogel structures, observing the deformation at printed interfaces and identifying regions of increased localized deformation for samples under uniaxial tension. Wyss et al. [21] performed DIC at both macro and micro scales to measure the local strain field of a cellulose/hydrogel composite under cyclic loading. The results uncovered the effects of cyclic loading on the local strain distribution.

Despite the above-mentioned studies, the accuracy of the DIC measurements of highly localized deformations in hydrogels has not been well quantified. Possible sources of inaccuracy include system alignment, quality of the optics, speckle pattern, and subset size [22–26]. The existence of large deformations and high strain gradients may exacerbate these issues. Thus, the accuracy of the method must be carefully examined before the measured results can be reliably applied to fracture problems. In prior works such as [18, 21], the DIC results are explored in a qualitative way. In other studies, strain contours obtained from DIC were qualitatively compared to FEM simulations [17] or the minimum/maximum strain values were compared [27]. To establish the accuracy of the methodology, more careful comparison between the experimental results and reliable numerical simulation is necessary. This is the prerequisite to apply DIC to obtain more reliable, quantitative information, such as experimentally measuring crack tip loading parameters for fracture mechanics applications.

In this study, we apply DIC to measure the localized deformation of PVA dual-crosslink hydrogel specimens with strain concentrations. The principal goals of this paper are to establish the accuracy of the DIC measurement for our material and setup, validate the measurements in cases of large strain gradients and to apply the results to prove a theoretical result predicted in our prior work, namely that the deformation fields in a cracked sample of the viscoelastic hydrogel are stationary during a stress relaxation test. A secondary goal is to provide guidance on practical aspects such as the optical setup, speckle pattern and DIC analysis.

We begin with a brief outline of the material synthesis. Details of the experimental setup are then discussed, including the preparation of the speckle pattern, the optical system, load application and validation of the test system. Details on the preparation and quality of the speckle pattern are discussed as these may be problematic for some hydrogels due to their high water content. The effects of DIC analysis parameters such as subset size and strain radius are discussed, and the method's accuracy is assessed against results from uniaxial tension and from geometries involving large strain gradients. After the accuracy of the method has been carefully validated, we apply DIC to the question of the time dependence of deformation fields in a cracked sample of the hydrogel during a stress relaxation test.

Methodology

The material in this study is poly (vinyl alcohol) (PVA) hydrogel crosslinked by transient (physical) and covalent (chemical) bonds. A brief summary of the synthesis can be found in supplementary information. More details can be found in [7].

Speckle Pattern Generation

Generating a high-quality speckle pattern is challenging for this type of hydrogel due to high water content of about 90%. Several techniques to generate speckle patterns have been explored by other researchers, such as spraying ink with an airbrush [19, 27, 28], powder deposition [16, 17, 29], marking using a marker pen [30], transfer from an inkjet-printed pattern on acetate to the gel [31] and embedding fluorescent or white light micro-beads [18, 20, 32, 33]. In some cases, the material has enough intrinsic contrast that no patterning is needed [34].

We explored airbrush spraying, powder deposition and using a marker pen and concluded that spraying black ink using an airbrush works best. This process can be performed in a short time period and the pattern can be consistently repeated. The primary challenge for airbrush spraying is that as the surface of the hydrogel mostly consists of water, the drying of the paint is slow and thus wet ink drops may coalesce or smear as shown in Fig. 1(a).

To generate a high-quality pattern using an airbrush, an ink that dries fast and has dark and opaque color is needed. In this research, after trying several different types of ink, we chose Koh-I-Noor RAPIDRAW ink. Patterns with very large speckles and a very high speckle density should be avoided, as those patterns are more likely to smear as shown in Fig. 1*a*. Finer, moderately dense speckles dry faster and do not smear. To obtain a fine pattern, a relatively high air pressure of 80 psi was supplied to an IWATA HP-C airbrush. A low flow of ink should be used, which can be achieved by adjusting the airbrush trigger during painting. To allow the spray to start to dry in flight, the airbrush should be held relatively far from the sample, about 0.6 m. During one stroke of the airbrush only a small number of particles are painted on the surface of the specimen. The density of the speckles can be controlled by the number of strokes. An example of a pattern we generated for this study is shown in Fig. 1(b). The quality of the pattern will be further assessed in section 3.

DIC Setup

We performed DIC with an in-house built experimental setup, Fig. 2. The mechanical loading was applied using a custom-built tensile tester. The hydrogel specimen was clamped between two aluminum grips. Sand paper sheets were glued to the inside of the grips to minimize sample slippage. The bottom grip was fixed to a base and vertical motion of the top grip was provided by a Zaber X-LSM200A-E03 translational stage. The linear motion resolution of the stage is 0.047625 μm. Load was measured by an Interface SMT1–1.1 load cell (4.9 N capacity) and displacement by an OMEGA LD620 LVDT.

Images for DIC measurements were acquired using a CCD camera (FLIR Grasshopper3 4.1 MP Mono) with a telecentric lens (Edmund Optics, SilverTL™ 0.16 ×). With this lens/camera system one pixel corresponded to 20 μm on the sample. Two LED lights were used to provide additional illumination. The whole experimental setup was fixed on an optical breadboard, as shown in Fig. 2. A telecentric lens was chosen since it has a very small distortion ratio and it helps to minimize the effects of out-of-plane motion and the non-perpendicularity between the specimen and optical axis. The strain errors due to both out-of-plane motion and non-perpendicularity are proportional to Z^{-1}, the inverse of the distance between the object and the plane of the lens [24, 35]. For a telecentric lens, the distance Z is characterized by an effective distance $Z_{\text{effective}}$, which is much larger than the physical distance Z. Thus, the above-mentioned errors can be significantly reduced.

DIC Software

The DIC software used in this study was Ncorr, an open source code written in MATLAB [36]. Ncorr utilizes the reliability guided DIC algorithm developed by Pan et al. [37]. To account for large deformation, instead of using a fixed reference image, the reference image is updated based on the correlation coefficient [38]. In the DIC analysis there are three key parameters that will affect the results: the subset radius, the radius in pixels of the circular subset used to correlate sub-images; the subset spacing, the spacing in pixels between neighboring subsets; and the strain radius. The strain radius

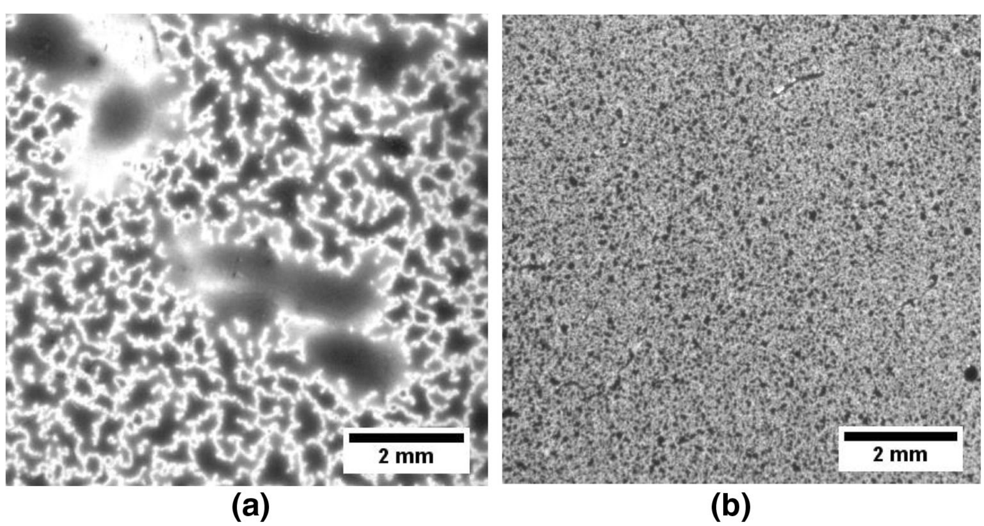

Fig. 1 Representative views of the speckle patterns (*a*) a low-quality pattern that smears (*b*) a high-quality pattern generated using an airbrush

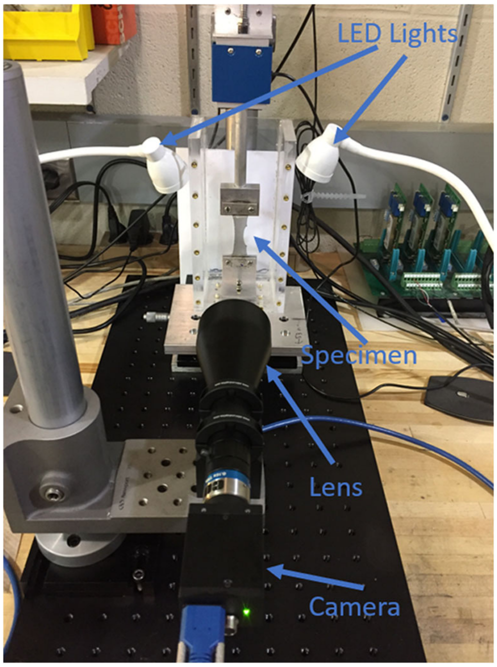

Fig. 2 Experimental setup for large strain testing of hydrogel and deformation measurement with DIC

represents the size of the region over which displacement data are fit to a plane in order to calculate the displacement gradient. The parameters used here for specific tests are stated in the relevant sections. More details on the code are available in [36] and at the website (http://www.ncorr.com/).

Convention for Deformation Measures

In this study, we follow the convention used in Ncorr. The horizontal (x direction) and vertical (y direction) displacements are denoted by U and V respectively. The stretch ratio, which is the current length divided by the original length, is denoted by λ. The strain measure used in this study is Lagrange strain tensor $\varepsilon^{\mathbf{Lag}}$, which is defined as $\varepsilon^{\mathbf{Lag}} = \frac{1}{2}\left(\mathbf{F}^{\mathrm{T}}\mathbf{F}-\mathbf{I}\right)$, with $\mathbf{F}$ being the deformation gradient and $\mathbf{I}$ the identity matrix. All the strains are viewed with respect to the reference (undeformed) configuration.

Validation under Homogeneous Deformation

Before applying DIC to measure localized strain involving strain concentration, we first validate the accuracy of the system under uniform deformation. There are several possible issues, including the quality of the speckle pattern, the alignment of the test setup, lens distortion, and sample slippage. In this section we discuss in detail here the quality of the speckle pattern and then validate the accuracy of the setup against uniaxial tension tests.

Quality of the Speckle Pattern

A high-quality speckle pattern is critical to an accurate DIC measurement. A basic requirement is that the pattern is mechanically robust: it does not smear or debond from the surface of the specimen under large deformation. This is usually not a problem for dry materials such as rubber. However, for some hydrogels with high water content, the water might seep from the surface of specimen and interact with the generated pattern. Thus, special attention must be paid to patterning such materials.

To test whether the speckle pattern is mechanically robust, we tested the speckle pattern under large deformation and multiple loading cycles. We preloaded the specimen to a stretch ratio λ of 1.2 then took a reference image. Here a pre-stretch λ of 1.2 is chosen as the reference configuration in order to avoid the possible issue of buckling upon unloading. Then we loaded the specimen from λ = 1.2 to

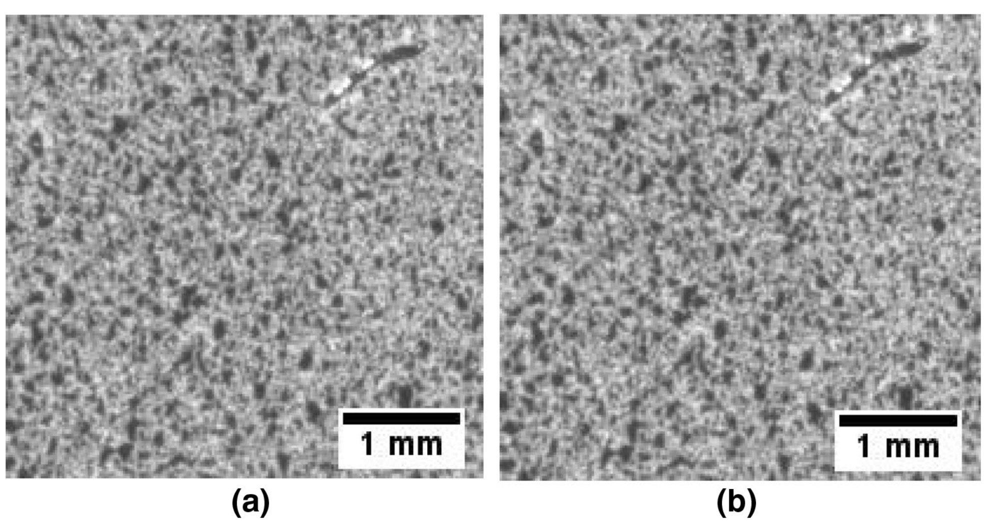

Fig. 3 The details of speckle pattern in a 4 × 4 mm region of interest. (**a**) reference image: taken before loading (**b**) current image: taken after the 8 cycles of loading from λ = 1.2 to 1.6. 1 pixel = 20 μm

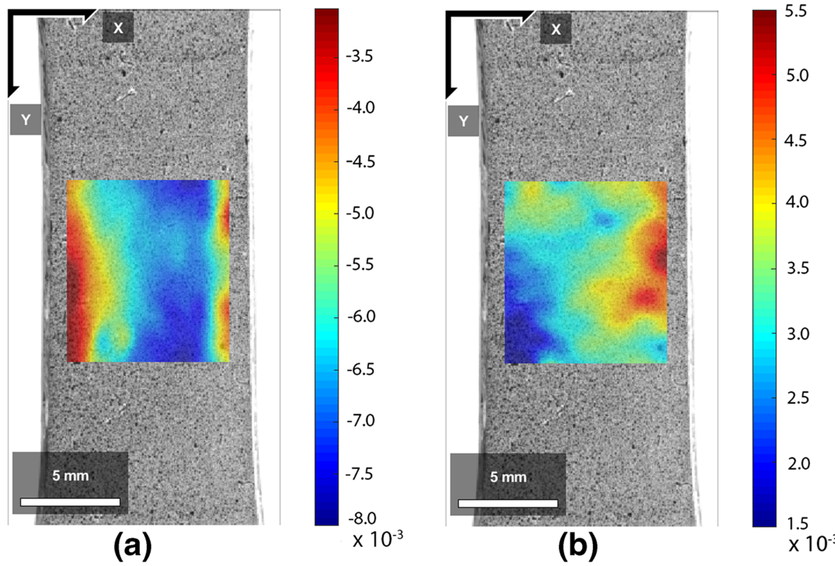

Fig. 4 The induced strains after 8 cycles of loading: (**a**) ε_{xx}^{Lag} (**b**) ε_{yy}^{Lag}

λ = 1.6 at $\dot{\lambda} = 0.05$/s and unloaded to the stretch of 1.2. This loading and unloading was repeated for 8 cycles. Then a second image was taken at λ = 1.2 (current image). After this, we carefully examined the pattern in the current image to confirm that the pattern was intact after cycles of loading. The details of the speckle pattern in a 4 × 4 mm region of interest in the reference and current images are shown side by side in Fig. 3. A careful examination of Fig. 3 confirms that the speckle does not show any visible change after the cyclic loading to large deformation. This is a first indicator of the robustness. To make further validation, DIC was applied to the in reference and current images and relative strains were obtained in a *region of interest* (ROI) of about 10 mm × 8 mm. A subset size of 35, a subset spacing of 2, and a strain radius of 5 were used. The strain results ε_{xx}^{Lag} and ε_{yy}^{Lag} are shown in Fig. 4. The average and standard deviation of the strains within the ROI are summarized in Table 1. It can be seen that the induced strain is on the order of 10^{-3}, very small relative to the strains we will apply to this gel. Thus, we concluded that the pattern is sufficiently durable for the purpose of this study.

Once the mechanical robustness has been confirmed, the quality of a speckle pattern can also be assessed based on other criteria, as proposed in [39–44]. However, no single global quantity accurately predicts the quality of the pattern in terms of its ability to yield accurate results [39]. We have computed the histogram, particle size distribution and the mean intensity gradient (MIG) [44]. Results are shown in the SI. A relatively high MIG was achieved, which indicates a desirable pattern according to [44]. The average particle size is 3.8 pixels, which is helpful to avoid aliasing effects [39], see SI.

Table 1 Statistical data for the strains within ROI for pattern durability test. Note that here at the reference configuration, the material is under a stretch λ of 1.2

Strain component	Expected value	DIC measurement
ε_{xx}^{Lag}	0	−0.0065 ± 0.0008
ε_{yy}^{Lag}	0	0.0030 ± 0.0006

Uniaxial Tension Loading

After the quality of the pattern has been verified, we further test the accuracy of our setup under relatively large deformation. We performed uniaxial tension tests on the hydrogel specimen. The speckle pattern was sprayed on a hydrogel specimen (35 mm gauge length, 12 mm width, 2 mm thickness) using the previously mentioned method. The specimen was loaded to a stretch ratio λ of 1.5 with images were taken at stretch intervals Δλ of 0.05. The images were analyzed using Ncorr (subset radius:35, subset spacing: 3, strain radius: 10).

In uniaxial tension, the non-vanishing Lagrangian strains are $\varepsilon_{xx}^{Lag} = \varepsilon_{zz}^{Lag} = \left(\lambda^{-1}-1\right)/2, \varepsilon_{yy}^{Lag} = \left(\lambda^{2}-1\right)/2$. For λ = 1.5, the corresponding strains are $\varepsilon_{xx}^{Lag} = -0.167$ and $\varepsilon_{yy}^{Lag} = 0.625$. The strain fields are shown as color contours in Fig. 5. It can be seen that the measured strains are very close to the applied strain. From Fig. 5, at first glance, it might seem that there is a great deal of non-uniformity in the strain distribution. But this impression is primarily due to the color scale of the plot. In order to better understand the strain distribution, we computed the average and standard deviation of strains in the ROI. The results are plotted in Fig. 6 for five different stretch levels, along with the theoretical results. From Fig. 6, it can be seen that the average strains in the ROI are very close to the theoretical values, and the strain values in the ROI have a very small deviation. The results indicate that our setup can generate

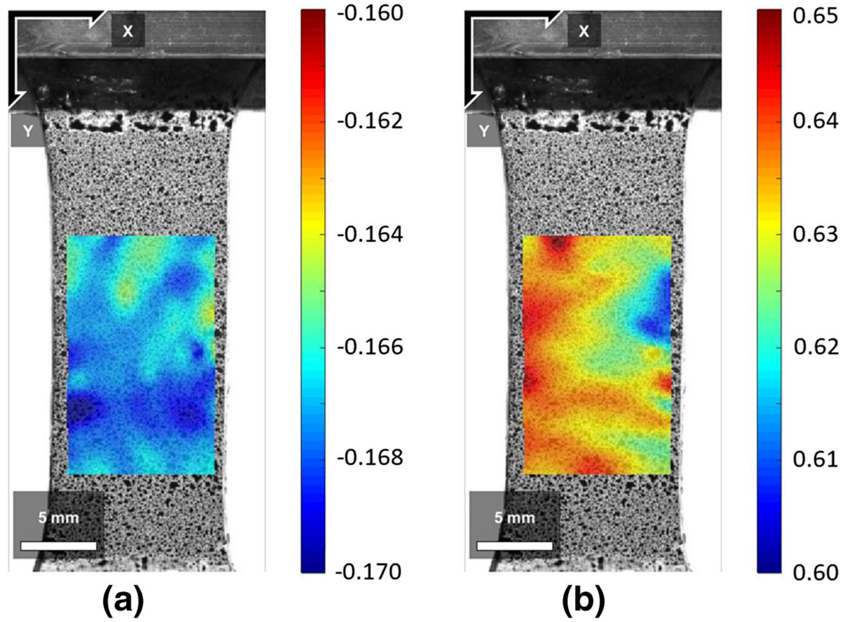

Fig. 5 The strain fields for the uniaxial tension test: (**a**) ε_{xx}^{Lag} (**b**) ε_{yy}^{Lag}

accurate results up to at least λ = 1.5. From the uniaxial tension tests, we also confirmed that grip slippage was not a significant problem at the current stretch level. If significant slippage existed, the measured strain in the y direction would be dramatically reduced and deviate from the theoretical value.

Validation of DIC in Hydrogels with High Strain Concentrations

After the reliability of the experimental setup has been checked, we applied DIC to several hydrogel specimens with strain concentrators. The goal is to test whether the current setup and method are able to accurately measure deformation with high strains and strain gradients. The DIC accuracy is established through quantitative comparison of DIC results to finite element simulation results. The FEM procedures and corresponding constitutive model has already been validated by detailed comparison of the FEM results to known, asymptotic stress and deformation fields for a plane-stress tensile crack in the hydrogel [11, 45].

Experiment

We applied DIC to hydrogel specimens with three different types of strain concentrators: a 4-mm -diameter central hole, a 5-mm-radius semi-circular edge notch and a 5 mm horizontal edge crack. The test geometries are sketched in Fig. 7. All the specimens are 17.5 mm in width, 2 mm in thickness and 33 mm in gauge length. Specimens of rectangular shapes were first cut using an X-ACTO blade. Then the stress concentrators were made using a steel punch for the circular hole and

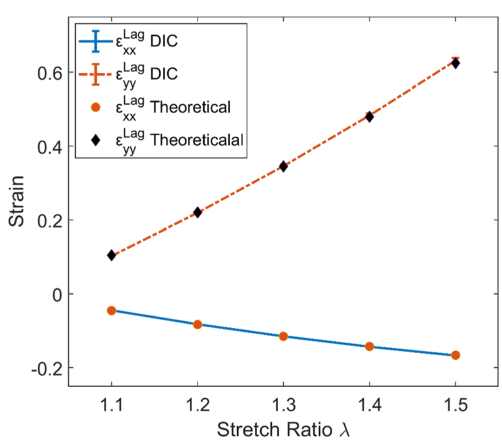

Fig. 6 Comparison between strains obtained from DIC (averaged over the ROI in Fig. 5) and theoretical values at different stretch levels. Here the standard deviation is very small, so the error bar is barely visible

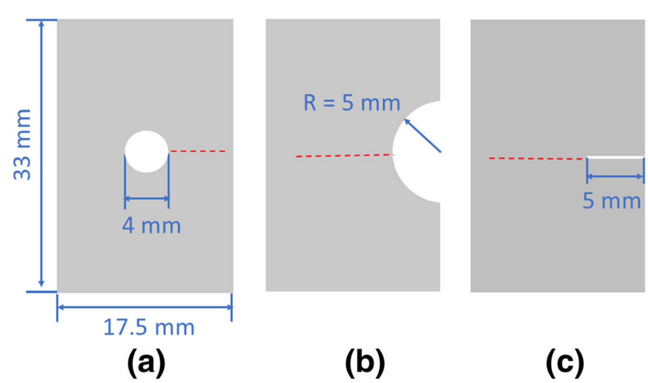

Fig. 7 Schematic view of the geometries of specimens: (**a**) circular hole (**b**) semi-circular edge notch (**c**) edge crack. The red dashed lines indicate the path on which the strain values from FEM and DIC are compared in Fig. 10

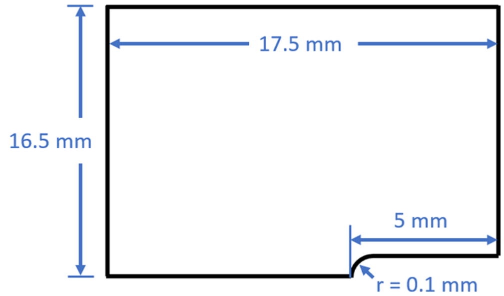

Fig. 8 Geometry used in FEM for the edge-cracked sample. The radius of the notch is exaggerated to show this feature

notch and a single edge razor blade for the crack. Then the specimen was loaded to a nominal stretch ratio of 1.5 at a stretch rate of 0.02/s. Images were acquired at a stretch interval $\Delta\lambda$ of 0.05. The images were analyzed using Ncorr. We used the following parameters: subset size: 30, subset spacing: 2, strain radius: 3. The choice of these parameters is discussed in section 4.3.2.

FEM Simulation

We carried out finite element simulations in ABAQUS using a plane stress material user-subroutine (UMAT), for a constitutive model developed for the PVA gel [9, 11]. Briefly, in our model, the gel consists of two independent networks: a chemically crosslinked network that does not break, and a physically crosslinked network that can break and heal. The total strain energy is the sum of the strain energies carried by the two networks. When a physical chain breaks, it loses all its strain energy, and it reforms at zero initial stress. Thus, the strain energy in the physical network is determined by the deformation experienced by the physical chain from its birth

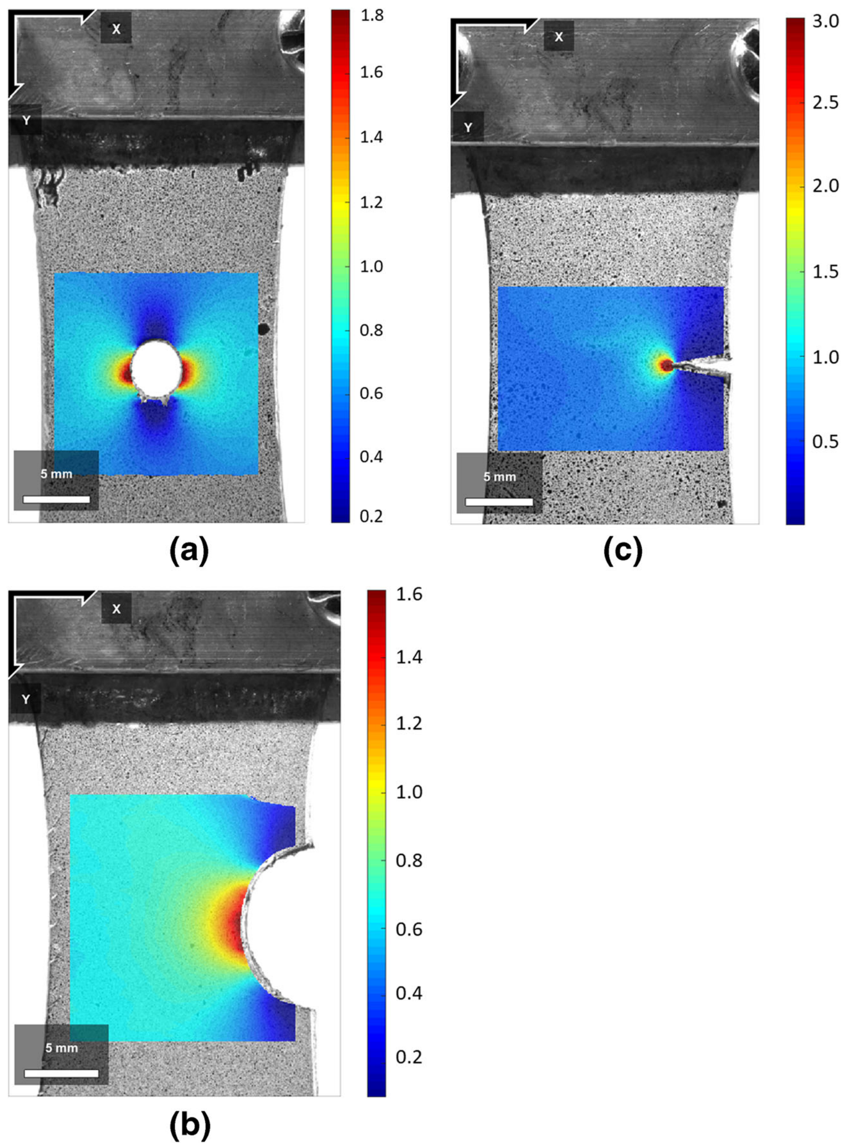

Fig. 9 ε_{yy}^{Lag} distribution for different geometries: (**a**) circular hole (**b**) semi-circular edge notch (**c**) edge crack. These contours are mapped onto the reference configuration

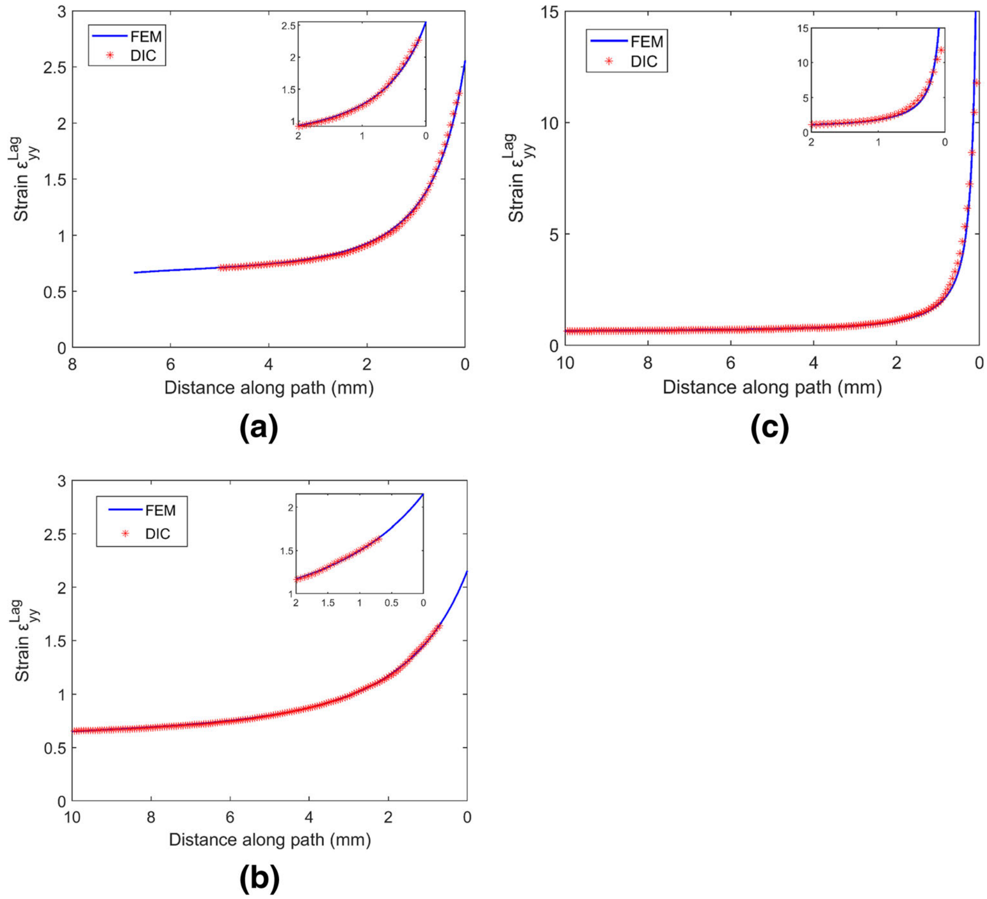

Fig. 10 Comparison between the ε_{yy}^{Lag} strain obtained from DIC and FEM along a specific path (Fig. 7) for the test geometries: (**a**) circular hole (**b**) semi-circular edge notch (**c**) edge crack. Insets show strains in the first 2 mm from the hole, notch or crack

(reattachment) at an earlier time, τ, to the current time, t. The resulting constitutive model captures the experimentally observed non-linear viscoelastic behavior of the gel. Our constitutive model is completely determined by four independent material parameters which can be fit using data from a relaxation test (detailed fitting process is discussed in [9]). Details of the model, material parameters and the tension and stress relaxation tests used to identify the model parameters are given in the SI.

We have implemented our constitutive model with the fitted material parameters, in ABAQUS using a plane stress UMAT to calculate the strain fields in the three different geometries shown in Fig. 7 [45]. We used quarter symmetry to model the specimen with a central hole, Fig. 7*a*, and half symmetry for the edge notched and edge cracked geometries, Fig. 7(b,c). The single edge blade we used to cut the sharp crack in Fig. 7(c) has a finite thickness (~ 0.1 mm), thus the crack tip in this geometry will also have a finite radius of curvature. To account for this finite notch radius, the sharp crack is modeled as a notch with a radius of curvature 0.1 mm at the tip, as shown in Fig. 8 below.

The smallest element sizes are 0.01, 0.01, and 0.001 mm for the three geometries in Fig. 7(a-c), respectively. All simulations are carried out using quadratic plane stress elements. Each sample is loaded at a constant stretch rate of 0.02/s for 25 s until the nominal stretch ratio reaches 1.5.

From the FEM results, we extract the nominal strains along the red dashed lines shown in Fig. 7. The nominal strain is defined as

$$\varepsilon^{N} \equiv \mathbf{V} - \mathbf{I} \tag{1}$$

where $\mathbf{V}$ is the left stretch tensor. It is related to the deformation gradient tensor by $\mathbf{F} = \mathbf{VR} \Rightarrow \mathbf{V} = \mathbf{FR}^{T}$, where $\mathbf{R}$ is the rotation tensor. Because the red dashed lines lie on the symmetry planes, the x and y directions are the principal directions, so $\mathbf{R} = \mathbf{I}$ and $\mathbf{V} = \mathbf{F}$. The deformation gradient along these symmetry planes is

$$\mathbf{F} = \varepsilon^{N} + \mathbf{I} \tag{2}$$

Thus, in the FEM analysis the Lagrangian strains can be calculated from the nominal strains as

$$\varepsilon^{\mathbf{Lag}} = \frac{1}{2}\left(\mathbf{F}^{T}\mathbf{F} - \mathbf{I}\right) = \frac{1}{2}\left[\left(\varepsilon^{N} + \mathbf{I}\right)^{T}\left(\varepsilon^{N} + \mathbf{I}\right) - \mathbf{I}\right]. \tag{3}$$

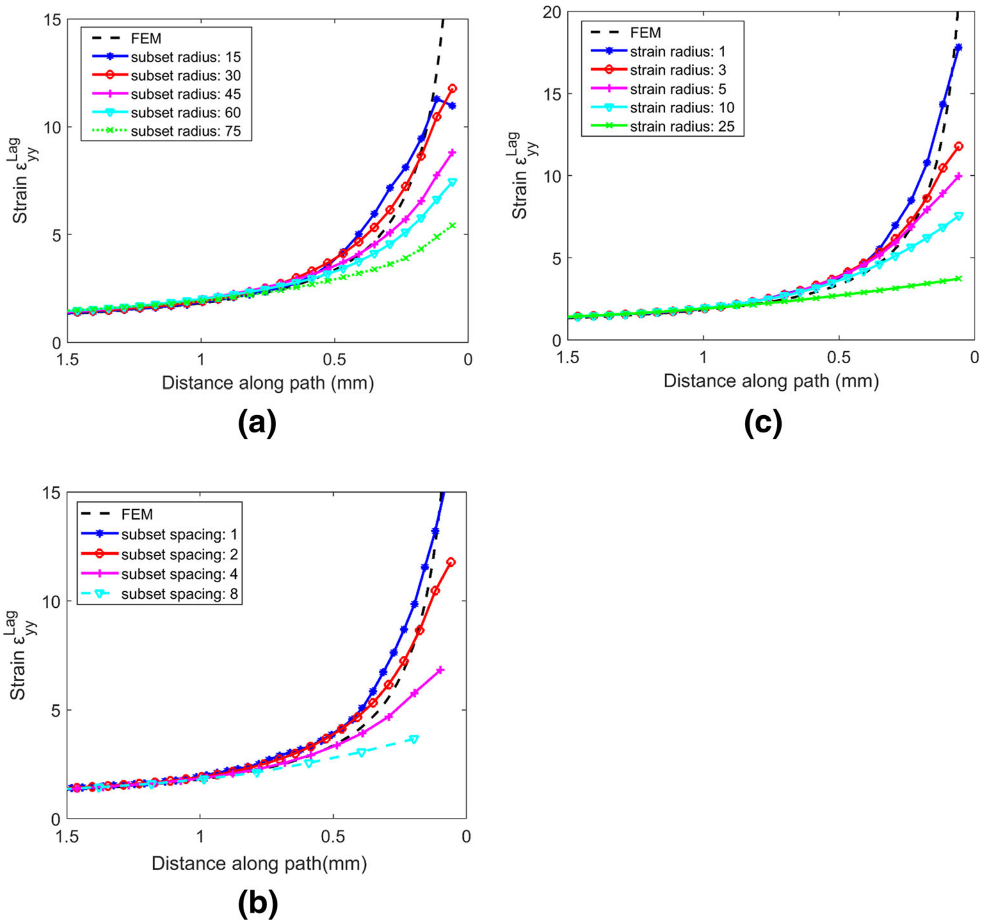

Fig. 11 Effects of different DIC parameters on the measured on the measured strain ε_{yy}^{Lag}: (**a**) subset size (**b**) subset spacing (**c**) strain radius

Results

Comparison Between DIC and FEM

We focus here on the strain components in the primary loading direction (y). The ε_{yy}^{Lag} strain distributions obtained from DIC

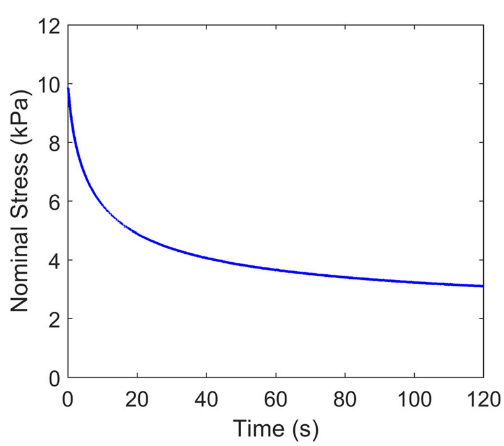

Fig. 12 The relaxation of nominal stress. Here the starting time t = 0 s is when the applied displacement stops increasing (relaxation starts)

for all different geometries are shown as color contours in Fig. 9. These results give a general idea of the strain distribution. To make a more rigorous comparison between strains obtained from DIC and FEM, we extracted the ε_{yy}^{Lag} strain values along a path extending from the strain concentrators (the red dashed lines in Fig. 7) from both FEM and DIC. The corresponding results are compared in Fig. 10. Note that very near the edges of those strain concentrators, the quality of the speckle pattern is poor. Thus we cannot use DIC to measure the deformation right up to these edges. From Fig. 10, it can be seen that for the primary loading direction (y direction), DIC was able to capture the sharp change of strains near the stress concentrators and that the values obtained from DIC are very close to those obtained from FEM. This detailed comparison establishes the accuracy of the current setup for the measurement of highly localized strains.

DIC parameters for strain analysis of crack tip fields

Due to the singular nature of the crack tip fields, DIC measurements of strain in this case are particularly sensitive to the

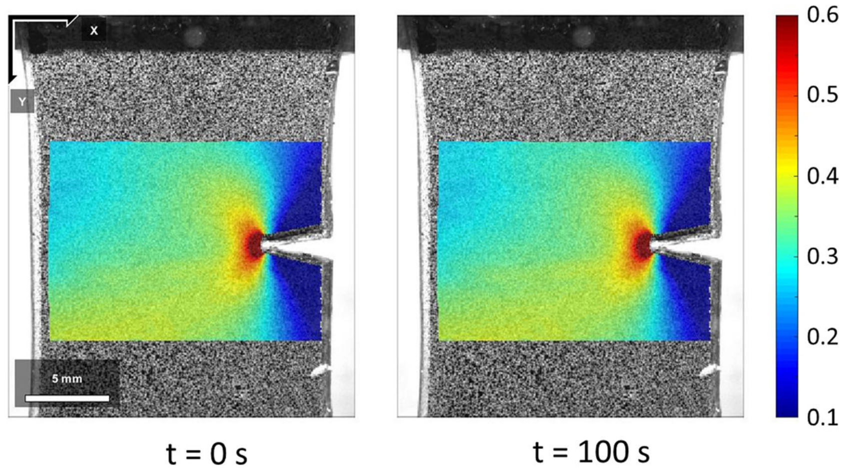

Fig. 13 The comparison of strain field ε_{yy}^{Lag} at time t = 0 s (relaxation started) and t = 100 s (after 100 s of relaxation)

DIC parameters. Here the effects of the choice of subset size, subset spacing and strain radius on the strain results are analyzed and discussed. With the parameters used in Figs. 9 and 10, (subset size:30, subset spacing: 2 and strain radius:3), we are able to obtain DIC results that agree well with the FEM simulation. However, the choice of these parameters requires some analysis.

First, we look at the subset size. Prior works on this topic [42, 46, 47] generally conclude that a larger subset is beneficial to a better correlation, at the cost of losing spatial resolution. A larger subset helps reduce the random error (noise) but can increase systematic error (bias). We processed the images from the edge-cracked sample using five different subset radii: 15, 30, 45, 60 and 75 pixels (with subset spacing of 2 and strain radius of 3 fixed). The resulting ε_{yy}^{Lag} values very close to the crack tip are shown in Fig. 11(a). Increasing the subset size decreases the peak strain measured by DIC. The effect of subset size is significant only in the region very close to the crack tip (~ 0.5 mm). Even closer to the crack tip (~ 0.1 mm), the theoretical strain is very high and even the smallest subset is unable to resolve this strain. The subset size of 15 is perhaps too small, which leads to an apparent error for the data point closest to the crack tip.

Next consider the subset spacing. Using a smaller subset spacing increases the spatial resolution which is critical to capturing the very high localized strain gradient. We tried different subset spacing: 1, 2, 4, 8 and 16 (with subset radius of 30 and strain radius of 3 fixed). For the largest subset chosen, 16, Nccor failed to generate meaningful results. Thus in Fig. 11(b) we compare results only for the first four subset spacings. It can be seen clearly that the measured strain peak decreases with increasing subset spacing.

The last parameter to discuss is strain radius. Ncorr calculates the strain by computing the displacement gradient. The displacement data are first fit to a planar surface and then the gradients are computed from the fitted planes. Increasing the strain radius means using a larger plane and thus increases the smoothing. The effects of different strain radius are shown in Fig. 11(c) (with subset radius of 30 and subset spacing of 2 fixed). Larger strain radii reduce the measured crack tip strains.

Based on the above analysis to best capture the singular strain near a crack, small values for subset size, subset spacing, and strain radius should be used, as long as this does not result in poor correlation or produce noisy results.

Application of DIC to Stress Relaxation of Hydrogel with Edge Crack

This PVA dual-crosslink hydrogel is highly viscoelastic. When a specimen is subject to a step displacement, the stress in the specimen decreases with time (stress relaxation). However, for a specimen with an edge crack, it is not clear whether the strain near the crack will also relax with time. In our previous study [11], we argue that the deformation

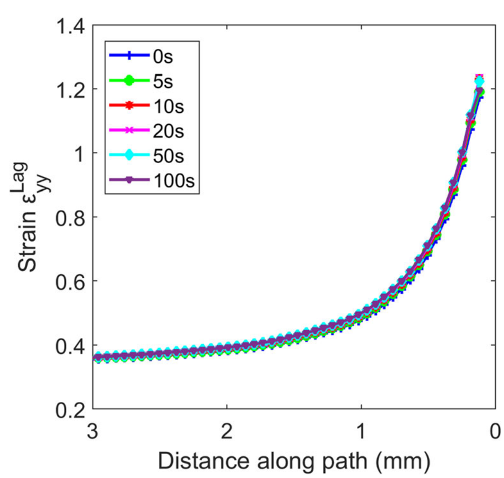

Fig. 14 The strain along a specific path (Fig. 7(c)) at different time steps during a stress relaxation test

gradient **F** at any point is independent of time in a stress relaxation test. Based on this argument, the strain field in a stress relaxation test should also be time independent, even though material shows significant viscoelasticity. In this section we experimentally validate this argument using DIC to map the strain field.

An edge-cracked hydrogel specimen with a geometry as in Fig. 7(c) was loaded to a stretch ratio λ of 1.3 at a stretch rate of 0.03/s. Then the stretch was held constant at 1.3. We started the image acquisition before the loading starts and images were taken every second for 200 s. Then these images were processed using Ncorr, with the following parameters: subset size: 30, subset spacing: 2 and strain radius: 3. In this way the strain distribution in the specimen at different time steps can be obtained. Here we loaded the specimen at $\dot{\lambda} = 0.03$/s instead of a higher stretch rate because a higher stress will be induced at a higher rate, and the specimen might fracture before the target stretch level is reached. However, even the specimen was loaded at slower loading rate, there's still a significant stress relaxation observed. The relaxation of the far-field nominal stress is plotted in Fig. 12. Here the far-field nominal stress is defined as the force measured divided by the uncracked cross-sectional area (17.5 mm × 2 mm). From Fig. 12, the far field stress dropped by about 50% of its initial value after 20 s and about 70% after 100 s. Although the stress field near the crack tip can't be directly measured, based on the relaxation of the far-field stress, the stress near the crack tip will also experience significant relaxation.

Now we look at the evolution of the strain with respect to time during a stress relaxation test. We first look at the strain distribution. We compared the strain field ε_{yy}^{Lag} at time t = 0 s (relaxation started) and t = 100 s (after 100 s of relaxation) in Fig. 13. From the strain contours in Fig. 13, it can be seen that there is no perceptible change of ε_{yy}^{Lag} with respect to time. To make a more detailed comparison, we extracted ε_{yy}^{Lag} along the same path as in Fig. 7*c*. And the strain profile at different time steps are plotted in Fig. 14. From Fig. 14, it can be seen that the strain remains stationary during the stress relaxation process, consistent with the argument made in ref. [11].

Conclusion

In this study, we applied 2D DIC to measure the deformation of a PVA dual-crosslink hydrogel in the presence of large strain gradients. The details of the experimental setup and several practical issues were discussed. In order to quantitatively validate accuracy, the experimental results were compared with results of finite element simulations based on a large deformation viscoelastic constitutive model developed in prior work. This comparison confirms the accuracy of DIC for measuring the high strain gradient of the specimen in the presence of large deformation. This is relevant for the study of fracture mechanics of such hydrogels. We further show that with a proper selection of DIC parameters, the current method can accurately capture the strain near a crack tip in tension. To better capture the singular strain field, smaller values for subset size, subset spacing and strain radius should be selected. Once the accuracy of the method was carefully validated, we used DIC to study the evolution of the crack tip strain field during a stress relaxation test. The results show that despite stress relaxation of over 70% the strain field remains stationary.

Acknowledgements This material is based upon work supported by the National Science Foundation under Grant No. CMMI -1537087.

References

1. Kwon HJ, Yasuda K, Gong JP, Ohmiya Y (2014) Polyelectrolyte hydrogels for replacement and regeneration of biological tissues. Macromol Res 22(3):227–235
2. Qiu Y, Park K (2001) Environment-sensitive hydrogels for drug delivery. Adv Drug Deliv Rev 53(3):321–339
3. Gong JP, Katsuyama Y, Kurokawa T, Osada Y (2003) Double-Network Hydrogels with Extremely High Mechanical Strength. Adv Mater 15(14):1155–1158
4. Webber RE, Creton C, Brown HR, Gong JP (2007) Large Strain Hysteresis and Mullins Effect of Tough Double-Network Hydrogels. Macromolecules 40(8):2919–2927
5. Henderson KJ, Zhou TC, Otim KJ, Shull KR (2010) Ionically Cross-Linked Triblock Copolymer Hydrogels with High Strength. Macromolecules 43(14):6193–6201
6. Sun TL et al (2013) Physical hydrogels composed of polyampholytes demonstrate high toughness and viscoelasticity. Nat Mater 12(10):932–937
7. Mayumi K, Marcellan A, Ducouret G, Creton C, Narita T (2013) Stress–Strain Relationship of Highly Stretchable Dual Cross-Link Gels: Separability of Strain and Time Effect. ACS Macro Lett 2(12):1065–1068
8. Long R, Mayumi K, Creton C, Narita T, Hui C-Y (2014) Time Dependent Behavior of a Dual Cross-Link Self-Healing Gel: Theory and Experiments. Macromolecules 47(20):7243–7250
9. Guo J, Long R, Mayumi K, Hui C-Y (2016) Mechanics of a Dual Cross-Link Gel with Dynamic Bonds: Steady State Kinetics and Large Deformation Effects. Macromolecules 49(9):3497–3507
10. Long R, Mayumi K, Creton C, Narita T, Hui C-Y (2015) Rheology of a dual crosslink self-healing gel: Theory and measurement using parallel-plate torsional rheometry. J Rheol 59(3):643–665
11. Guo J et al. (2018) Fracture mechanics of a self-healing hydrogel with covalent and physical crosslinks: A numerical study, Journal of the Mechanics and Physics of Solids
12. Liu M, Guo J, Hui C-Y, Creton C, Narita T, Zehnder A (2018) Time-temperature equivalence in a PVA dual cross-link self-healing hydrogel. J Rheol 62(4):991–1000
13. Pan B, Qian K, Xie H, Asundi A (2009) Two-dimensional digital image correlation for in-plane displacement and strain measurement: a review. Meas Sci Technol 20(6):062001
14. Khoo S-W, Karuppanan S, Tan C-S (2016) A Review of Surface Deformation and Strain Measurement Using Two-Dimensional Digital Image Correlation, Metrology and Measurement Systems, vol. 23, no. 3

15. Schreier H, Orteu J-J, Sutton MA (2009) Image Correlation for Shape, Motion and Deformation Measurements. Springer US, Boston
16. Kwon HJ, Rogalsky AD, Kovalchick C, Ravichandran G (2010) Application of digital image correlation method to biogel. Polym Eng Sci 50(8):1585–1593
17. Sasson A, Patchornik S, Eliasy R, Robinson D, Haj-Ali R (2012) Hyperelastic mechanical behavior of chitosan hydrogels for nucleus pulposus replacement—Experimental testing and constitutive modeling. J Mech Behav Biomed Mater 8:143–153
18. Leibinger A et al (2016) Soft Tissue Phantoms for Realistic Needle Insertion: A Comparative Study. Ann Biomed Eng 44(8):2442–2452
19. Hong Y, Sarntinoranont M, Subhash G, Canchi S, King MA (2016) Localized Tissue Surrogate Deformation due to Controlled Single Bubble Cavitation. Exp Mech 56(1):97–109
20. Christensen K, Davis B, Jin Y, Huang Y (2018) Effects of printing-induced interfaces on localized strain within 3D printed hydrogel structures. Mater Sci Eng C 89:65–74
21. Wyss CS, Karami P, Bourban P-E, Pioletti DP (2018) Cyclic loading of a cellulose/hydrogel composite increases its fracture strength. Extreme Mech Lett 24:66–74
22. Haddadi H, Belhabib S (2008) Use of rigid-body motion for the investigation and estimation of the measurement errors related to digital image correlation technique. Opt Lasers Eng 46(2):185–196
23. Pan B, Yu L, Wu D, Tang L (2013) Systematic errors in two-dimensional digital image correlation due to lens distortion. Opt Lasers Eng 51(2):140–147
24. Sutton MA, Yan JH, Tiwari V, Schreier HW, Orteu JJ (2008) The effect of out-of-plane motion on 2D and 3D digital image correlation measurements. Opt Lasers Eng 46(10):746–757
25. Jerabek M, Major Z, Lang RW (2010) Strain determination of polymeric materials using digital image correlation. Polym Test 29(3): 407–416
26. Hoult NA, Andy Take W, Lee C, Dutton M (2013) Experimental accuracy of two dimensional strain measurements using Digital Image Correlation. Eng Struct 46:718–726
27. Goh CP, Ismail H, Yen KS, Ratnam MM (2017) Single-step scanner-based digital image correlation (SB-DIC) method for large deformation mapping in rubber. Opt Lasers Eng 88:167–177
28. Moerman KM, Holt CA, Evans SL, Simms CK (2009) Digital image correlation and finite element modelling as a method to determine mechanical properties of human soft tissue in vivo. J Biomech 42(8):1150–1153
29. Horst CR, Brodland B, Jones LW, Brodland GW (2012) Measuring the Modulus of Silicone Hydrogel Contact Lenses. Optom Vis Sci 89(10):1468–1476
30. Dicker MP, Bond IP, Rossiter JM, Faul CF, Weaver PM (2015) Modelling and Analysis of pH Responsive Hydrogels for the Development of Biomimetic Photo-Actuating Structures, MRS Proceedings, vol. 1718
31. Subhash G, Liu Q, Moore DF, Ifju PG, Haile MA (2011) Concentration Dependence of Tensile Behavior in Agarose Gel Using Digital Image Correlation. Exp Mech 51(2):255–262
32. Mac Donald K, Ravichandran G (2019) An Experimental Method to Induce and Measure Crack Propagation in Brittle Polymers with Heterogeneities, in *Fracture, Fatigue,* Failure and Damage Evolution*, Volume* 6, pp. 21–23
33. Alshehri AM, Wilson OC, Dahal B, Philip J, Luo X, Raub CB (2017) Magnetic nanoparticle-loaded alginate beads for local micro-actuation of in vitro tissue constructs. Colloids Surf B: Biointerfaces 159:945–955
34. Skulborstad AJ, Wang Y, Davidson JD, Swartz SM, Goulbourne NC (2013) Polarized Image Correlation for Large Deformation Fiber Kinematics. Exp Mech 53(8):1405–1413
35. A. Hijazi, A. Friedl, and C. J. Kähler, "Influence of camera's optical axis non-perpendicularity on measurement accuracy of two-dimensional digital image correlation," vol. 5, no. 4, p. 10, 2011
36. Blaber J, Adair B, Antoniou A (2015) Ncorr: Open-Source 2D Digital Image Correlation Matlab Software. Exp Mech 55(6): 1105–1122
37. Pan B (2009) Reliability-guided digital image correlation for image deformation measurement. Appl Opt 48(8):1535
38. Pan B, Dafang W, Yong X (2012) Incremental calculation for large deformation measurement using reliability-guided digital image correlation. Opt Lasers Eng 50(4):586–592
39. Dong YL, Pan B (2017) A Review of Speckle Pattern Fabrication and Assessment for Digital Image Correlation. Exp Mech 57(8): 1161–1181
40. Crammond G, Boyd SW, Dulieu-Barton JM (2013) Speckle pattern quality assessment for digital image correlation. Opt Lasers Eng 51(12):1368–1378
41. Hua T, Xie H, Wang S, Hu Z, Chen P, Zhang Q (2011) Evaluation of the quality of a speckle pattern in the digital image correlation method by mean subset fluctuation. Opt Laser Technol 43(1):9–13
42. Lecompte D et al (2006) Quality assessment of speckle patterns for digital image correlation. Opt Lasers Eng 44(11):1132–1145
43. Park J, Yoon S, Kwon T-H, Park K (2017) Assessment of speckle-pattern quality in digital image correlation based on gray intensity and speckle morphology. Opt Lasers Eng 91:62–72
44. Pan B, Lu Z, Xie H (2010) Mean intensity gradient: An effective global parameter for quality assessment of the speckle patterns used in digital image correlation. Opt Lasers Eng 48(4):469–477
45. Guo J, Hui CY, Liu M, Zehnder AT (2019) The stress field near the tip of a plane stress crack in a gel consisting of chemical and physical cross-links, Submitted to Proceedings of the Royal Society A
46. Pan B, Xie H, Wang Z, Qian K, Wang Z (2008) Study on subset size selection in digital image correlation for speckle patterns. Opt Express 16(10):7037
47. Yaofeng S, Pang JHL (2007) Study of optimal subset size in digital image correlation of speckle pattern images. Opt Lasers Eng 45(9): 967–974